EE

GSI

GSI-94-71
PREPRINT
November 1994

SEPARATION OF ACTINIDE-MADE TRANSURANIA BY A GAS-FILLED MAGNETIC SEPARATOR

V. Ninov, P. Armbruster, F. P. Heßberger, S. Hofmann,
G. Münzenberg, Y. Fujita, M. Leino, A. Lüttgen

Gesellschaft für Schwerionenforschung mbH
Postfach 110552 · D-64220 Darmstadt · Germany

Separation of Actinide-made Transurania by a Gas-filled Magnetic Separator

V. Ninov *, P. Armbruster, F.P. Heßberger, S. Hofmann, G. Münzenberg,

Gesellschaft für Schwerionenforschung mbH, Postfach 110552, D-64220-Darmstadt, Germany

Y. Fujita,

College of General Education, Osaka University, Toyonaka, Osaka 560, Japan

M.Leino,

Accelerator Laboratory, University of Jyväskylä, P.O. Box 35, FIN-40351 Jyväskylä, Finland

A. Lüttgen.†

Rheinische-Friedrich-Wilhelms-Universität Bonn, Nussallee 14–16, D-53115 Bonn, Germany

October 27, 1994

GSI, Darmstadt, Germany

*E-mail adress: nase@VSCN.GSI.DE

†Deceased on January, 6th, 1993

Abstract

The performance of the gas-filled magnetic separator HECK at the UNILAC at GSI Darmstadt is described. The system consists of a 30°-dipole magnet and a quadrupole doublet of wide aperture. The separator is operated with helium at pressures between (0.1-1) hPa. It is used to investigate heavy ion induced fusion products in-flight. The recoils emerging from a thin target are separated with high efficiency of (10-50)%. The suppression factor of primary beam particles and transfer products is (10^{15}) and (10^{3}), respectively.

In this application of a gas-filled separator to synthesize transuranium elements using ^{238}U-targets, isotopes of the elements fermium and nobelium were identified in irradiations with ^{16}O- and ^{20}Ne-beams.

Introduction

For long, magnetic separators have contributed to the investigation of nuclear reaction products and their decay properties. In heavy ion reactions slow recoils show broad velocity and ionic charge distributions, thus magnetic rigidities spread over a wide range. This results in a wide spatial distribution of the recoils at the focal plane of a separator. The separation of the products emerging from a thin target may be achieved by combining electric and magnetic fields as this was realized in the velocity filter SHIP [1] and its post-separator NASE [2,3]. An alternative method applied here [4] uses a magnetic deflection system filled with low pressure gas. In the gas the recoils undergo atomic collisions. They lose and capture electrons, and take a trajectory determined by an average magnetic rigidity given by the average ionic charge. This separation technique, originally proposed by C.B. Fulmer and B.L. Cohen [5] and improved by P. Armbruster et al. [6,7], was successfully applied to the separation of fission fragments. For the study of evaporation residues from fusion reactions, V. Karnaukhov [8] and A. Ghiorso [9] developed gas-filled magnetic separators.

In this paper we report on the performance and the separation characteristics of the helium–filled magnetic–separator HECK, a HElium Charge-exchange Kaleidoscope, installed from 1989 to 1991 behind the velocity filter SHIP at GSI, Darmstadt, and its application to the successful separation of actinide isotopes produced in fusion reactions of light projectiles, O and Ne, with the actinide target ^{238}U.

Dedicated gas-filled separators for the study of isotopes of heavy elements have been installed and are operated now at Dubna, Russia [10], Jyväskylä, Finland [11] and Osaka, Japan [12].

Separation of fusion products with a gas–filled separator

Due to full momentum transfer in complete fusion reactions of heavy ions, the recoils emerging from the production target have a well defined velocity with a narrow distribution ($\Delta v/v \leq 0.2$) peaked at the velocity of the compound velocity and an angular distribution peaked in beam–direction. Reaction products from other reaction channels, such as transfer and elastic collisions, have smaller masses and atomic numbers and larger velocities.

Ions with the mass m and the velocity v, passing through a homogeneous magnetic field region with the flux density B will follow a trajectory with the radius ρ. The magnetic rigidity $B\rho$ of an ion in Tm is given by the following equation,

$$B\rho = 0.02267 \cdot A\frac{v/v_0}{q} \quad ,$$

where the velocity is perpendicular to B expressed in units of the Bohr velocity v_0=2.19 $\times$ 10^6 m/s and $B\rho$ equals the ratio of its momentum over its ionic charge. Heavy ions penetrating through a gas-filled region are slowed down, undergo atomic charge-changing collisions and suffer from small angle multiple scattering. In the magnetic field they follow trajectories determined by the mean value of momentum over charge. If the mean free path of an ion between two charge-changing collisions is short compared to the length of its total trajectory, i.e. the number of charge-changing collisions is large, then the mean charge state is well defined and the fluctuation around the mean value will be small. To outline the features of the gas–filled separator we will use the Bohr predictions [17] for the mean charge. Derived from the Thomas–Fermi model of the atom the mean charge can be expressed by

$$\overline{q} = (\frac{v}{v_0}) \cdot Z^{1/3}$$

for a velocity range $1 < v/v_0 < Z^{2/3}$.

The magnetic rigidity can be rewritten as

$$B\rho = 0.02267 \cdot \frac{A}{Z^{1/3}} \; Tm.$$

In first order, the corresponding trajectories in the gas are determined by the mass and atomic number only and become independent from the initial charge and velocity distribution. For numerical calculations of ionic charge distributions and cross sections for charge–changing collisions in helium one has to rely on semiempirical formulas proposed by the authors of following references [9, 13–16].

HECK was built to demonstrate that a gas-filled separator can be a useful tool in studies of very asymmetric fusion reactions producing evaporation residues with Z>90 at production cross sections smaller than 1μb. Its performance is characterized by

- a good transport efficiency,
- a sufficient suppression of all other, abundantly produced reaction products,
- a spot size in the focal plane, where the desired reaction products are collected, allowing the use of position sensitive Si-detectors.

The resolution of the gas-filled separator is determined by the ion optical dispersion of the system and the width of the spatial distribution of the collected events in the focal plane. This width depends on the following quantitities [7, 9]:

- statistics of charge-exchange collisions in the gas filling,
- small angle multiple scattering in the gas,
- fluctuations of the mean charge due to a velocity dispersion,
- beam and target size at the target position,
- the ion optical aberrations.

Beam and target size as well as contributions from ion optical aberrations are negligibly small ($\sim$ 1 cm) compared to the dominating atomic processes.
Measurements and a Monte Carlo simulation allowed to test the performance and are described in the next sections.

The Spectrometer.

The DQQ-spectrometer HECK installed at the central beam line behind the velocity filter SHIP is sketched in Fig.1. A magnetic dipole is followed by a magnetic quadrupole doublet the characteristics of which are given in table 1. The total path length is 3.85 m. The large apertures of the quadrupoles allow for an acceptance of $\Omega = 10$ msr. The dispersion of the system at the focal plane is 6.1 mm for a 1% change in $B\rho$.

Dipole		Quadrupoles	
deflection angle	30°	–	–
inclination of pole edges	30°	yoke–length	500 mm
deflection radius	1.396 m	–	–
gap	90 mm	aperture–radius	110 mm
max. flux density	1.6 T	max. field gradient	9 T/m
max. current	625 A	–	625 A

Table 1: Technical specifications of the magnets of the recoil separator HECK.

The entrance window of 15 mm diameter (100 μg/cm^2 of graphite) is mounted in front of the target chamber. It separates the gas-filled part from the high vacuum beam-line. A current grid is used for determining the beam profile and alignment. Beam current is measured by a Faraday cup. Both devices are mounted in front of the entrance window in vacuum. The primary beam, having passed the target, is dumped at the chamber wall inside the dipole chamber.

The system is filled with helium at a pressure of (0.01–1) hPa. The gas enters near the target position and is pumped out at the detector box. The pressure of the gas supply is reduced by a mechanical throttle valve. A constant flow is set by an electromagnetically operated valve. An exhaust throttle valve which is a step-motor driven butterfly valve, determines the amount of gas which flows through the system. The pressure of the gas is measured by a capacitance pressure sensor. The dc-output signal of the pressure sensor is used to set the position of the exhaust valve.

The detector system is installed in the gas-filled section. At the focal plane of HECK a 24 x 60 mm^2 passivated ion implanted silicon detector, divided into ten strips (In-

tertechnique IPS 24 x 60-300N10), is mounted to register energy, position and time of the incoming particle and to measure the subsequent radioactive decay of the implanted particles. The average resolution of each strip is 20 keV for 5 MeV α-particles.

Monte Carlo simulation of the trajectory in gas-filled magnetic systems

A semi-microscopic model for the calculation of the trajectory of slow ($v \approx \alpha c$) heavy ions in gas-filled magnetic systems has been developed. We consider charge–exchange processes, multiple small–angle scattering, and kinetic energy–loss of the ions passing through gaseous media combined with first order ion optical calculations. The trajectory of an ion is governed by the Lorentz force exerted on the ion in a homogeneous magnetic field. We calculate the trajectory by integrating the equation of motion of the ions including a term which takes into account the slowing down of the ions. The interaction with the gas is incorporated in the calculations by introducing the mean free path λ between two collision processes. The probability ω for an ion to survive a flight path s without any collisions is given by the relation:

$$\omega(s) = exp\left(-\frac{s}{\lambda}\right)$$

The probability ω is sampled with random numbers between 0 and 1 using a standard Monte Carlo algorithm. At each vertex an interaction with a neutral He–atom is chosen and the integration is continued. The mean free path λ is related to the cross section σ by the relation $\lambda = 1/n\sigma$. Here n denotes the number of atoms/cm^3 in the gas and $\sigma = \sum_i \sigma_i$ is the total cross section. The index i denotes the capture, loss, or multiple scattering cross section. The simulations are carried out by transporting a large number of incoming recoils to the focal plane with randomly sampled coordinates and cross sections. The energy and position spectra are accumulated by collecting the coordinates (x_j, y_j) of the ions reaching the focal plane and hitting the detector.

Determination of the interaction parameters

a) Energy loss. An ion passing the gas-filled region is slowed down. At velocities $v > v_o$ electronic stopping dominates. The stopping power S describes the overall action of all elastic and inelastic ion-electron collisions including energy losses from charge–exchange and multiple scattering events, which contribute to the slowing down of the motion of the ion. Between two atomic collision events the motion is governed by the equation of motion in a magnetic field

$$m \cdot \frac{dv}{dt} \cdot \frac{\vec{v}}{v} = q(\vec{B} \times \vec{v}) - S \cdot \left(\frac{\vec{v}}{v}\right) \quad .$$

Besides the Lorentz force the stopping force $S \cdot \vec{v}/v$ appears in the equation of motion. Between two vertices the charge state is well-defined and stays constant, but both forces depend on its value. The stopping force scales with q^2. Its value is calculated from the average stopping power S.

$$S = \bar{S} \cdot \left(\frac{q}{\bar{q}}\right)^2$$

The average stopping power is taken from energy-loss tables [18], the mean ionic charges from Ref. [14].

b) Charge–exchange. The cross sections for electron capture and loss of an ion strongly depend on the velocity, on the atomic number of the gas, and on the charge state of the ion. Moreover, calculations assume that the ion is in its ground state, which is only true if the time between two collisions is long enough to allow deexitation. There are very few experimental data on cross sections. We determined the total cross section σ_0 by a simple measurement. It follows from the slope of a semilogarithmic plot of the yield of a defined charge state with pressure. We choose $\bar{q} = 4$. For the simulation the total cross section is approximated as a sum of the cross sections for electron capture and loss, and represented by an exponential function.

$$\sigma_c(q) \;=\; \sigma_0/2 \times exp(\; a_c \cdot (q - \bar{q}))$$

$$\sigma_l(q) \;=\; \sigma_0/2 \times exp(-a_l \cdot (q - \bar{q}))$$

The ionic charges are assumed to follow a normal distribution, the variance of which is taken from [13]. The values of $\bar{q}$ have been taken from [14], and the parameters a_c

and a_l were fitted to data obtained for heavy ions with velocities close to the Bohr velocity v_0 and taken from [13]. Only one-electron transfer processes are considered. Multiple transfer is neglected, as for low velocities the cross sections for multiple electron capture and ionization are much smaller than single-electron transfer cross sections. Experimental data [15, 16] confirm this assumption for ions with $v/v_0 \sim 1$. The values of the total cross section in this energy range are of the order of the Bohr cross section $\pi a_0^2 = 0,9 \cdot 10^{-16}$ cm$^2 \sim 100$ Mb.

c) Multiple scattering. The multiple small-angle scattering acts on the trajectory of an ion by rotating the velocity vector of the recoils in space in each vertex through an angle Θ. Θ is sampled with a normal distribution

$$F(\Theta) = (2\pi \cdot \sigma_\Theta^2)^{-1/2} \cdot exp- \left(\frac{\Theta^2}{2 \cdot \sigma_\Theta^2} \right)$$

with σ_Θ the standard deviation. The width (in the following called FWHM) of the angular distribution is calculated using the multiple scattering formalism of Meyer [19] and Sigmund [20, 21].

Measurements and simulations testing the performance.

a) Resolution. In Fig.2 we present the measured spatial distribution of Ac-isotopes from the reaction ^{22}Ne + ^{197}Au at two pressures. The distribution of well defined charge states at p=10^{-2} hPa is totally smeared out at 0.5 hPa.

In Fig.3 the evolution of the focal plane spectra with pressure is simulated for ^{217}Ac. The spectrum at low pressures shows discrete peaks reflecting the charge distribution of the recoils emerging from the target, which is calculated using the formalism of Schlachter [22] for ions having penetrated solid foils. With increasing pressure the charge distribution changes gradually from the distribution at the exit from the solid target to the distribution in helium, which is characterized by a smaller average charge state.
In the region 10^{-2} hPa the charge states are still discrete and almost remain at positions of the initial distribution. These ions did not suffer from any charge-changing

collisions. However, between the discrete charge states some events are observed. These satellite events are attributed to ions having undergone charge–changing collisions inside the dipole, as verified in the experimental distribution, Fig.2. The charge distribution is far from being equilibrated, even at 10^{-1} hPa equilibration is not yet observed. The highest pressure shown, 0.5 hPa, is the optimal pressure showing the best resolution observed for the separation of ^{217}Ac. The peak is narrow but shifted to the left indicating the smaller average charge value in helium. The velocity dispersion of nearly 20% of the ions leaving the target induces only a small dispersion of the mean charge values. The contribution to the resolution is small and neglected.

Figure 4b illustrates the measured dependence of the width of the focal plane spectra defined as $\Delta(B\rho)/B\rho$ in % on the He-pressure for three different reactions leading to different isotopes with different velocities.

The width is decreasing with pressure until multiple small-angle scattering starts to increase the width again. The smaller the velocities of the recoils the smaller the optimal filling pressure. At $v=0.9v_0$ the pressure amounts to 0.3 hPa, whereas at $v=2.2v_0$ a pressure of 0.6 hPa is optimal. The width of the distribution increases from 6% at $v=2.2v_0$ to 18% at $v=0.9v_0$. With a dispersion constant of 6.1 mm/%, a FWHM of more than 11 cm follows for $v=0.9v_0$. Not to lose more than 10% of all events, the detector size should be as large as 20 cm for this most asymmetric reaction investigated. Figure 4a shows the vertical image size as a function of the pressure. For low pressures the width is almost constant. It reflects the contributions from beam and target size. The increase at higher pressure reflects the contribution from multiple scattering. In the simulation we found a FWHM-value of 26 mrad for the mean multiple scattering angle to reproduce best the vertical image size.

The mass resolution is determined from the FWHM of the focal plane spectra measured at optimum He-pressure for evaporation residues. The ionic charge of compound nuclei in He at low velocities ($v/v_0 \sim 1$) is constant and the velocity of the evaporation residues from complete fusion reactions is kinematically well defined as

$$v_{CN} = v_p \cdot \frac{A_p}{A_p + A_t} \ .$$

Thus, the width of the $B\rho$-distribution for an isotope produced in a fusion reaction depends only on the ion optical and atomic contributions discussed earlier. With a well defined $v/\bar{q}$-ratio the mass–resolution $\Delta A/A$ of a gas-filled separator for evap-

oration residues at low velocities equals the FWHM of the relative $B\rho$-width.

Figure 5 presents the position spectrum registered for the (^{22}Ne+^{208}Pb)-reaction. All masses lighter than the fusion products are found at smaller Bρ-values. A mass–resolving power $A/\Delta A$ of 8.3 follows from the distribution. The FWHM-value for the group of target-like nuclei at $A \sim 210$ is smaller than for the fusion products at $A \sim 225$. As their velocity is twice the velocity of fusion products the FWHM is reduced. The distance of 10% between the peaks reflects the mass and velocity difference, both entering the Bρ-values.
We have chosen He as a filling gas, as the suppression of ionic charge states with $q < 3$ leads to higher $\overline{q}$–values compared to H_2. The distribution of the ionic charge is cut-off at the lowest charge-values ($q < 3$), thus the final $B\rho$–distribution is narrower and in the average is shifted to smaller $B\rho$-values than in H_2. This allows a more compact construction of the separator.
The resolution is slightly better in He, than for H_2–gas–filling.
The suppression of target–like recoils scattered down to velocities close to those of the evaporation residues is in He very poor, as the average charges of target-like nuclei become similar to those of the evaporation residues. For that case H_2 filling shows a definitive advantage, which is exploited in recent experiments in Dubna [23]. As demonstrated in Fig. 5, the suppression of target-like nuclei is sufficient to reach cross section levels in the order of 10^{-33}cm^2.

b) Suppression of primary beam and recoils from nuclear reactions. Besides fusion evaporation residues, elastically scattered projectiles, target-like nuclei, and products from multinucleon transfer reactions may pass through the separator and reach the focal plane.
A typical spectrum measured in the focal plane is shown in Fig.6. As an analysis of the spectrum shows, the beam projectiles are suppressed by a factor of 10^{15}. The rejection of target-like products is smaller, of the order of $10^2 - 10^3$, as shown in Fig.5. Table 2 summarizes our results on suppression factors, as measured for the different reactions investigated.

c) Separation efficiency. The product of the transmission probability times the detection probability in the focal plane defines the separation efficiency.

Reaction	Target thickness	Suppression Factors	
		scatt. Projectiles	Transfer products
$^{16}O+^{208}Pb$	90 $\mu g/cm^2$	7.4×10^{16}	1.4×10^3
$^{22}Ne+^{208}Pb$	310 $\mu g/cm^2$	3.2×10^{15}	3.4×10^2
$^{22}Ne+^{209}Bi$	320 $\mu g/cm^2$	3.2×10^{15}	1.7×10^2
$^{40}Ar+^{208}Pb$	310 $\mu g/cm^2$	1.6×10^{10}	4.5×10^2

Table 2: Suppression factors for some typical reactions studied with the gas–filled separator.

On the one hand the transmission is an ion optical property of the system, on the other hand it depends on the properties of the beam, the collision kinematics, and the deexcitation processes having produced the evaporation residue to be detected. The transmission was measured directly for different deexcitation channels. Table 3 shows the results for different xn-reactions. Values between 12% and 42% for O^{16} and ^{40}Ar induced fusion reactions are obtained. The mass asymmetry of the collision partners $A_{Proj.}/A_{target}$ is the dominant parameter. The αxn-reactions show a smaller transmission and are suppressed compared to xn-reactions by more than one order of magnitude.

Reaction	Target thickness	Efficiency (%)
$^{197}Au(^{16}O,4\text{-}5n)^{208,209}Fr$	90 $\mu g/cm^2$	13 ± 1
$^{208}Pb(^{16}O,3\text{-}4n)^{220,221}Th$	90 $\mu g/cm^2$	12 ± 2
$^{197}Au(^{22}Ne,4\text{-}5n)^{214,215}Ac$	90 $\mu g/cm^2$	19 ± 3
$^{208}Pb(^{22}Ne,4\text{-}5n)^{225,226}U$	90 $\mu g/cm^2$	18 ± 3
$^{118}Sn(^{40}Ar,5\text{-}6n)^{152,153}Er$	720 $\mu g/cm^2$	42 ± 1
$^{164}Dy(^{40}Ar,6\text{-}7n)^{196,197}Po$	320 $\mu g/cm^2$	39 ± 4

Table 3: Transport efficiencies for HECK for xn-evaporation channels.

The detection efficiency depends on the detector size. For the most asymmetric reaction investigated here ($^{16}O + ^{238}U$) the FWHM amounts to 11 cm for the horizontal distribution in the focal plane and to 6 cm in the vertical direction. A detector

assembly detecting more than 80% ought to be used in order to keep the total separation efficiencies above the 10% level. Fig. 7 shows the focal plane position spectra for the reaction $^{40}Ar + ^{164}Dy$ in horizontal and vertical direction.
A simulation reproduces the measured spectra reasonably well. In this case the detector system used shows nearly no losses.
In Fig.8 we compare the efficiencies of HECK determined for different collision systems with corresponding values from SHIP. Evidently, for actinide-based fusion reactions - due to the larger solid angle of HECK (10 msr) compared to SHIP (2.5 msr) - the more efficient recoil separator suited for actinide-based reactions with 4 or 5 emitted neutrons is the gas-filled separator. The efficiency of HECK for actinide-based reactions nearly meets the value obtained with SHIP for Pb-based reactions. Identification of any transuranic fusion evaporation residue produced by xn-reactions is possible now using either SHIP or its HECK.

Identification of Fm- and No-isotopes from (^{16}O, $^{20}Ne + ^{238}U$)-reactions.

The high evaporation residue cross section $\sigma \sim 1\mu b$ [24] makes the reaction ^{238}U-(^{16}O,xn)$^{254-x}Fm$ well suited for investigation of the separation characteristics of HECK for actinide-based reactions. The well known α–decay properties of the Fm-isotopes guarantee an unambiguous identification. Figure 9a shows the energy spectrum registered in the beam-off time. The two main deexcitation-channels, 4n and 5n leading to $^{250,249}Fm$ and their daughters are seen. The long-lived daughter $^{246}Cf(T_{1/2}=36h)$ is clearly identified in the spectrum taken during 30 hours after end of irradiation (Fig. 9b).
The projectile beam at full energy is suppressed by a factor 10^{16} and a 9.8% separation efficiency is measured. None of the long–lived transfer products could be identified. Thus, the important suppression factor for transfer products could not be measured. The production cross sections of ^{250}Fm and ^{249}Fm equal 0.96 μb [24] and 0.46 μb, respectively.

As a next step towards heavier elements we investigated the reaction $^{238}U(^{20}Ne,xn)$-$^{258-x}No$ at 5.7 MeV/u. In the literature there are no cross section values published,

but the α-decays of ^{254,253}No are known. Figure 10 presents spectra accumulated within and out of the beam pulses with an integral dose of $1.3 \cdot 10^{15}$ projectiles. In the spectrum within beam pulses α-lines in the range (7-8) MeV are seen.
The α-group near 6 MeV is a left-over from a previous irradiation. The peak between 3 MeV and 4 MeV stems from evaporation residues (8.8 MeV) and scattered target recoils. Below 1 MeV β-particles and noise are registered. The isotopes ^{253}No and ^{254}No are clearly identified in the pause spectrum (insert of Fig. 10) together with their daughters and a grand-daughter ^{245}Cf. ^{253}No is produced with a cross section of (13±6)nb. No contaminant α-decays from transfer reactions are seen in the pause-spectrum.

Conclusions.

The performance of HECK demonstrates that for synthesis reactions of heavy elements using actinide targets the gas-filled separator is a competitive device. The main advantages are the full suppression of the primary beam and a 10% total separation efficiency even for the most asymmetric fusion reactions. The small focal plane image size of $\approx$ 60 mm allows the use of position-sensitive implantation detectors for decay-chain analysis. The sufficient suppression of transfer products allows detection of evaporation residues with production cross sections down to the 1 nb level without any ambiguities in the isotope identification as demonstrated in our experiments. Single α-chain analysis down to the few pb-level should be reliable if the daughters in the decay-chain are known even in a considerable background of transfer products. With a beam current of 2 pμA, 0.3 mg/cm^2 target thickness, and 10% total efficiency of separation an effective luminosity of $10^{30}\ cm^{-2} \cdot s^{-1} \approx 10^{-1} pb^{-1} d^{-1}$ for reactions producing superheavy elements can be envisaged. The successful application of the technique in recent experiments at Dubna [23], in which new isotopes of seaborgium (Z=106) and hassium (Z=108) were produced, demonstrates the strength of the method in SHE-research. The family of recoil separators is now able to efficiently separate and to unambiguously detect the fusion products from any heavy element synthesis reaction.

References

[1] G. Münzenberg, W. Faust, S. Hofmann, P. Armbruster, K. Güttner, H. Ewald, Nuclear Instruments and Methods 161, (1979), 65

[2] G. Berthes
Dissertation, GSI Report 87-12,(1987)

[3] F.P. Heßberger, G. Münzenberg, P. Armbruster, G. Berthes, W. Faust, S. Hofmann, W. Reisdorf, K.-H. Schmidt, H. Ewald, K. Güttner,
Lecture Notes in Physics 317, (1988), 289

[4] V. Ninov
Dissertation TH Darmstadt (1992), GSI Rep. 92-19, ISSN 0171-4546

[5] C. B. Fulmer, B. L. Cohen
Phys. Rev. 109, (1958), 94

[6] P. Armbruster
Nukleonik 3, (1961), 188

[7] P. Armbruster, J. Eidens, J.W. Grüter, H. Lawin, E. Roeckl, K. Sistemich, Nuclear Instruments and Methods 91, (1971), 504

[8] V.A. Karnaukhov, L. Rubinska, G. Ter-Akopian, V. Titov, V.A. Curgeev, JINR Dubna P13-4454,(1969)

[9] A. Ghiorso, S. Yashita, M.E. Leino, L. Frank, J. Kalnins, P. Armbruster, J.-P. Dufour, P.K. Lemmertz
Nucl. Instr. & Meth., A269, (1988), 194

[10] Yu.A. Lazarev, Yu.V. Lobanov, Yu.Ts. Oganessian, V.K. Utyonkov, F.Sh. Abdulin, G.V. Bulkanov, B.N. Gikal, S. Iliev, A.N. Mezentsev, A.N. Polyakov, I.M. Sedykh, I.V. Shirokovsky, V.G. Subbotin, A.M. Sukhov, Yu.S. Tzyganov, and V.E. Zhuchko,
R.W. Lougheed, K.J. Moody, J.F. Wild, E.K. Hulet, and J.H. McQuaid
Proc. Int. School-Seminar on Heavy Ion Physics, Dubna 1993 JINR-Report No. E7-93-274, Dubna, 1993 Vol.2, p. 497

[11] M. Leino, J. Uusitalo, T. Enqvist, K. Eskola, A. Jokinen, K. Loberg, W.H. Trzaska, J. Äystö,
Z. Phys. A 348,(1994), 151

[12] H. Miyatake, T. Nomura, H. Kawakami, J. Tanaka, M. Oyaizu, K. Morita, T. Shinozuka, H. Kudo, K. Sueki, Y. Iwata
Nucl. Instr. & Meth., B26, (1987), 309

[13] H. D. Betz
Rev. Mod. Phys.,44,(1972), 465

[14] A.-B. Wittkower, H.D. Betz,
Phys. Rev. A, 7, (1973), 166

[15] H. Knudsen, H.K. Haugen, P. Hvelplund,
Phys. Rev. A23, (1981), 600

[16] G.D. Alton, L.B. Bridwell, M. Lucas, C.D. Moak, P.D. Miller, C.M. Jones, Q.C. Kessel, A.A. Antar, M.D. Brown,
Phys. Rev. A23, (1981), 1073

[17] N. Bohr,
Phys. Rev. 59, (1941), 270

[18] L.C. Northcliffe, R.F.Schilling,
Nucl. Data Tables,A7,(1970), 233

[19] L. Meyer
Phys. Stat. Sol., b 44, (1970), 253

[20] P. Sigmund, J. Heinemeier, F. Bessebacher, P. Hvelplund,
Nucl. Instr. & Meth., 150, (1978), 221

[21] P. Sigmund,
Lecture Notes, Fysik Institut, Odense Universitet, 1990,

[22] A.S. Schlachter, J.W Stearns, W.G. Graham, K.H. Berkner, R.V. Pyle J.A. Tanis,
Phys. Rev., A27,(1983), 3372

[23] Y. Oganessian ,
Proc. of the Int. Conf. "Nucleus-nucleus Collisions" Taormina, Italy 5/30, (1994)

[24] N. Shinohara, S. Usuda, S. Ichikawa, T. Suzuki, M. Magara, H. Okashita, H. Yoshikawa, T. Horiguchi., Y. Iwata, S. Shibata, I. Fujiwara,
Phys. Rev., C34,(1986), 911

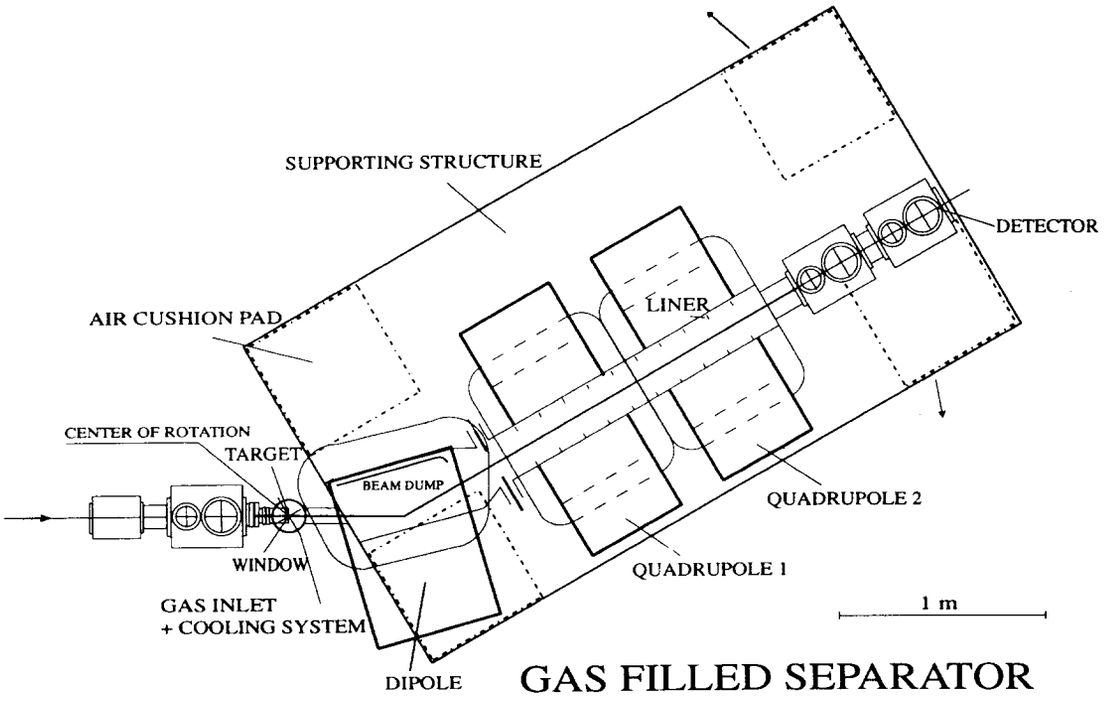

Figure 1: Top view of the gas-filled separator HECK. The whole system is filled with helium. The pressure is monitored by a capacitive gauge and kept constant within 0.001 hPa. The entrance window - 100 $\mu g/cm^2$ thick carbon foil, placed between the target chamber and a valve, separates the gas–filled region from the high vacuum beam-line.

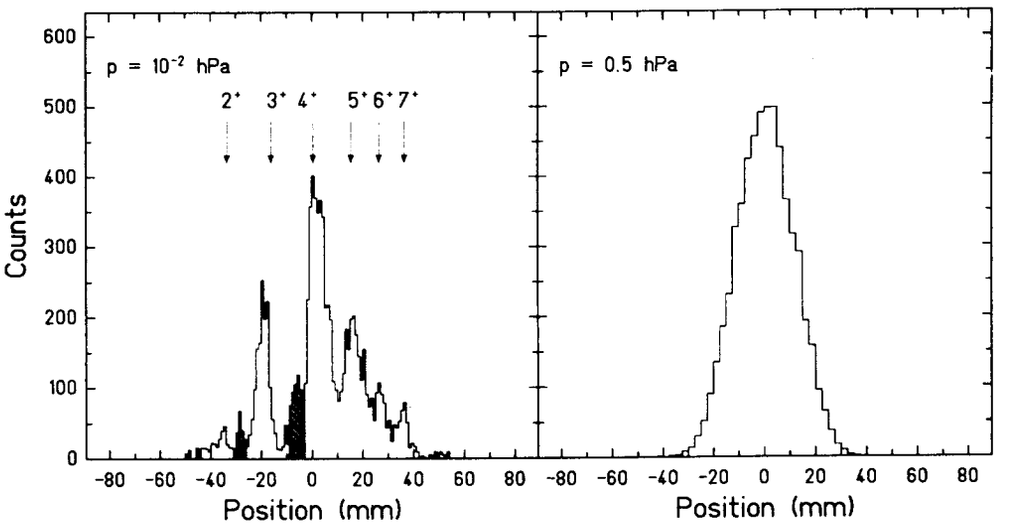

Figure 2: Measured focal–plane position spectra for ^{217}Ac recoils with an incident energy of E=14.5 MeV measured with HECK at different pressures. The hatched areas denote the satellite peaks mentioned in the text.

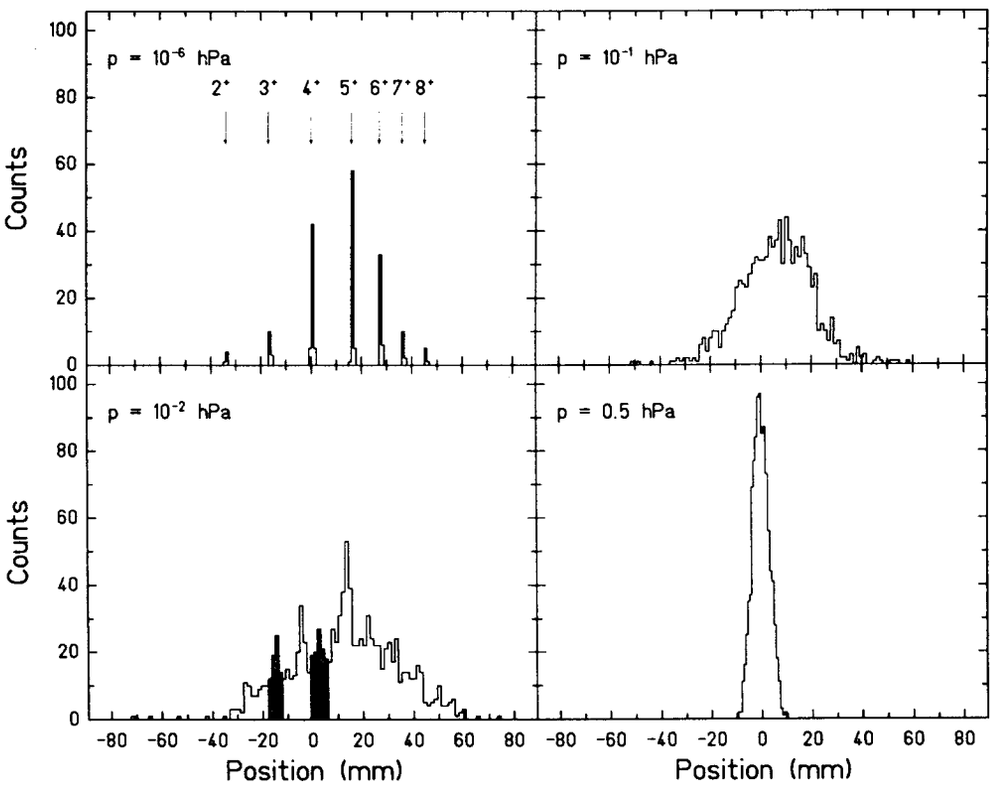

Figure 3: Position spectra calculated as described in the text for ^{217}Ac ions with an incident energy of E=14.5 MeV along the focal plane of the gas-filled separator. Note the shift in position of the mean value towards smaller q-values due to energy loss in the gas.

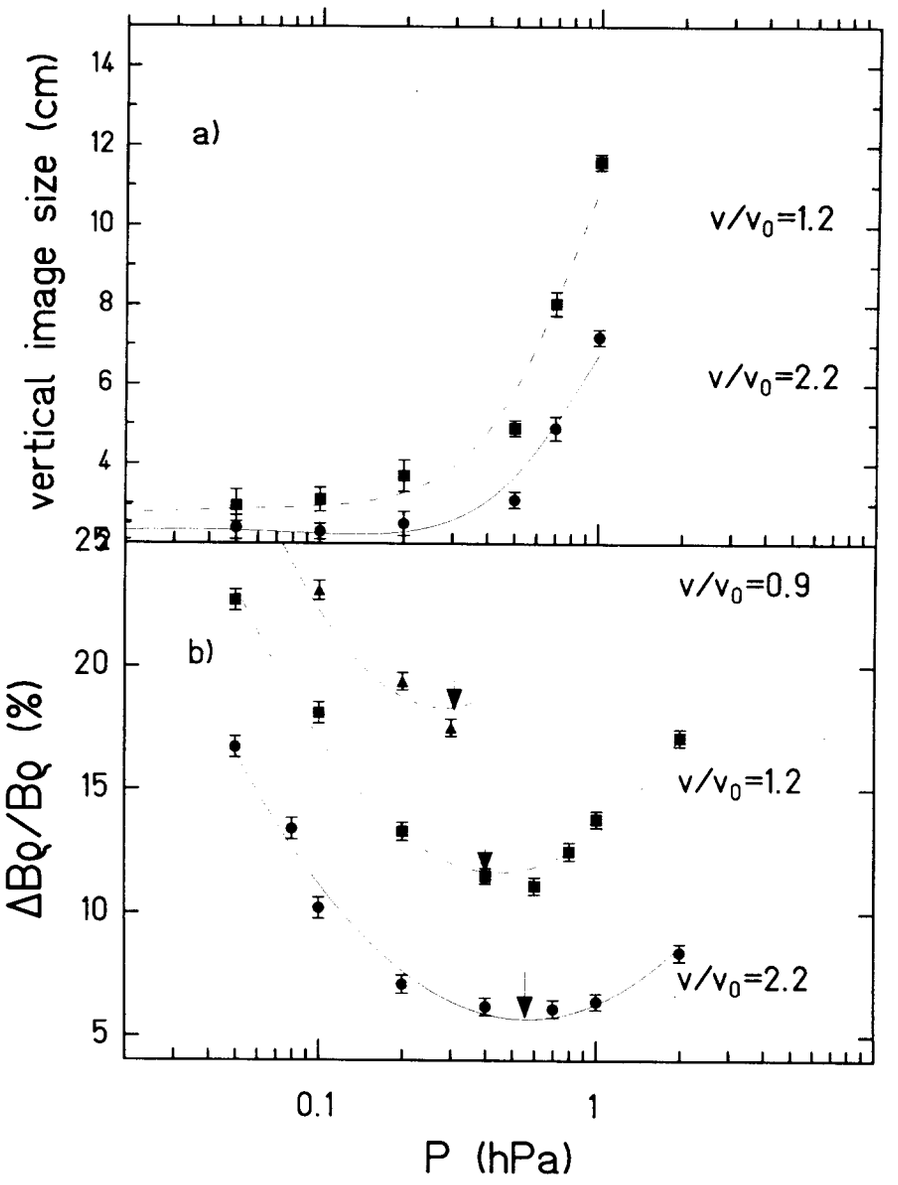

Figure 4: Experimental dependence of the horizontal and vertical image size in the focal plane of the gas-filled separator, which represents the $\Delta(B\rho)/B\rho$-resolution as function of the He-pressure. The values on the ordinate were taken from FWHM-values of the focal plane spectra. The lines represents the result of the calculated width of the distribution. The arrows denote the minimum of the image size corresponding to optimum pressure conditions.

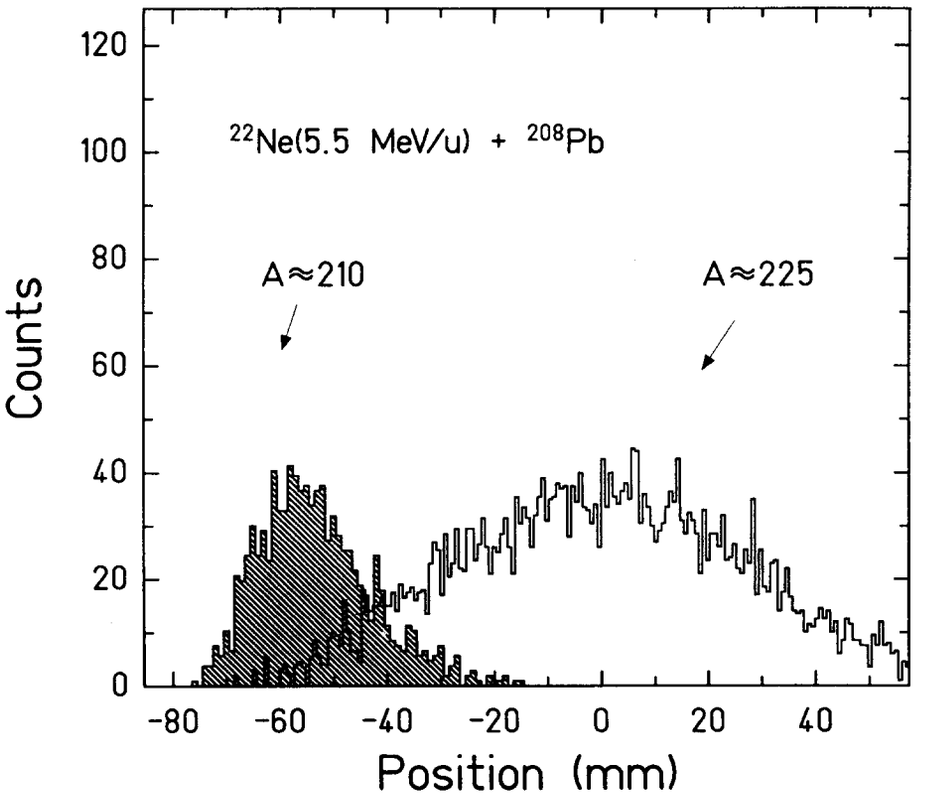

Figure 5: Focal-plane position spectrum obtained in the reaction ^{22}Ne+^{208}Pb. The hatched area represents the distribution of target–like nuclei with A$\sim$210. The distributions are evaluated from α-correlated events.

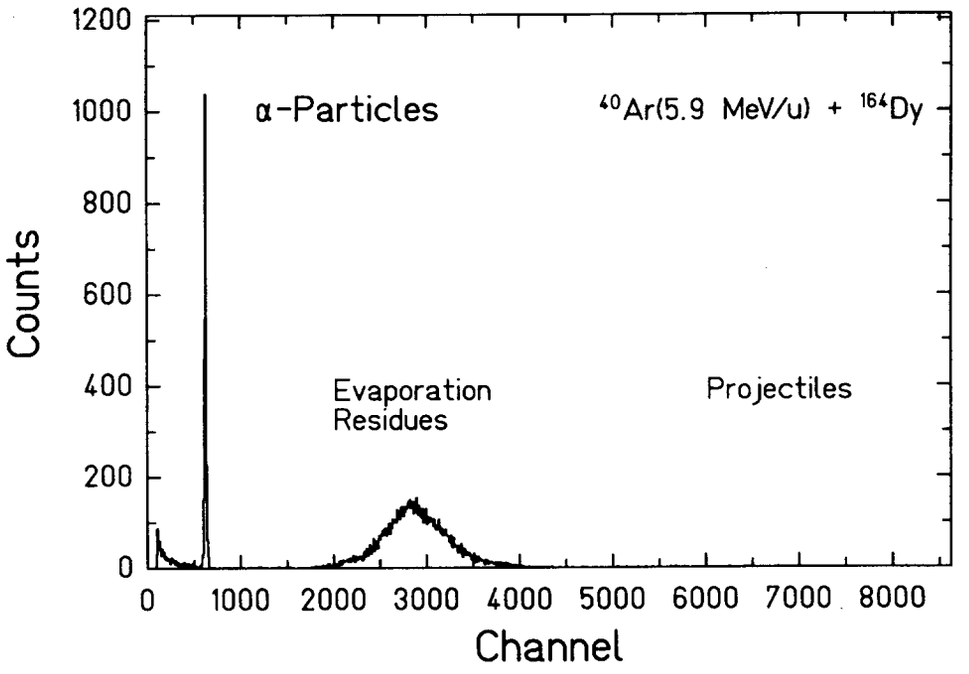

Figure 6: Energy spectrum of implanted particles for the reaction ^{40}Ar+^{164}Dy measured in the focal plane of the gas-filled separator at p=0.7 hPa. No time windows are set. The primary beam is completely suppressed.

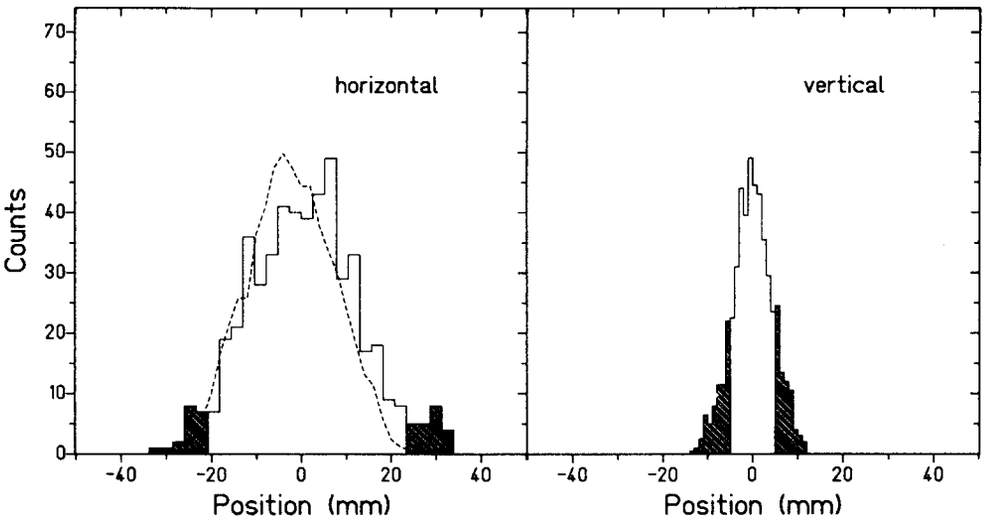

Figure 7: Position spectra for the reaction ^{40}Ar+^{164}Dy obtained with the focal plane detector of the gas–filled separator at p=0.7 hPa. To measure the vertical distrubution (right hand side of the picture) the detector is rotated by 90°. The hatched area represents the part cut by the detector size.

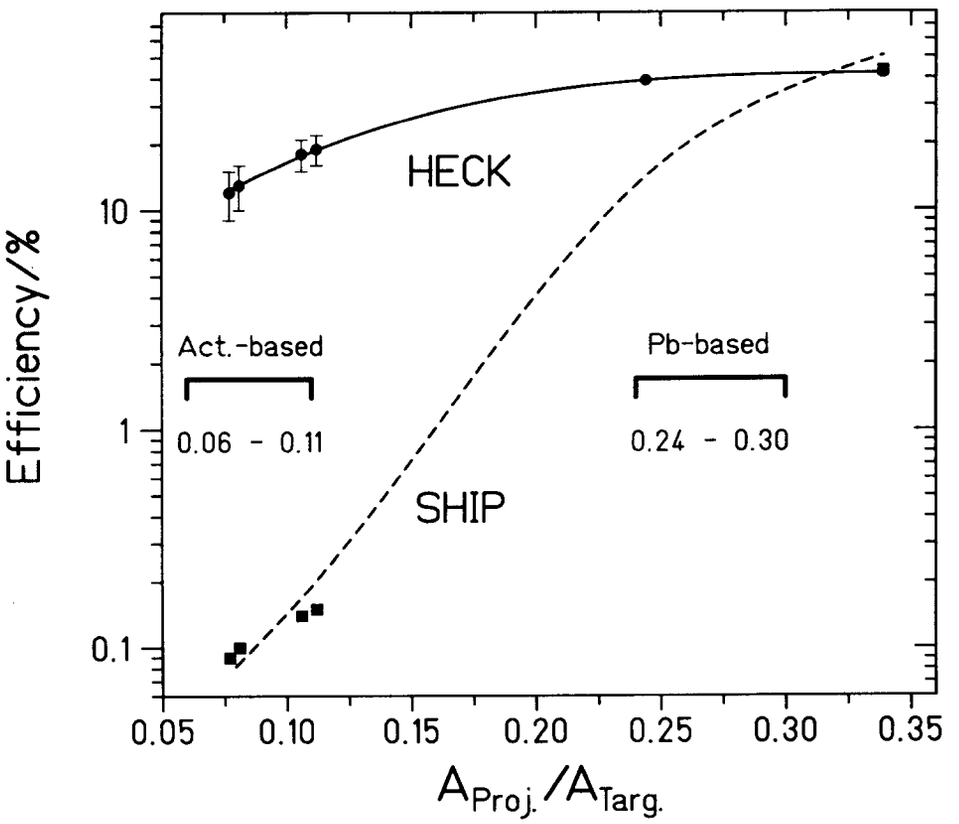

Figure 8: Detection efficiencies obtained for the velocity filter SHIP and for the gas-filled separator HECK as a function of the ratio of projectile to target mass. Recently, the solid angle of SHIP was increased from 2.5 msr to 3.8 msr. Its efficiency for 4n and 5n evaporation channels now is larger, compared to the dashed curve.

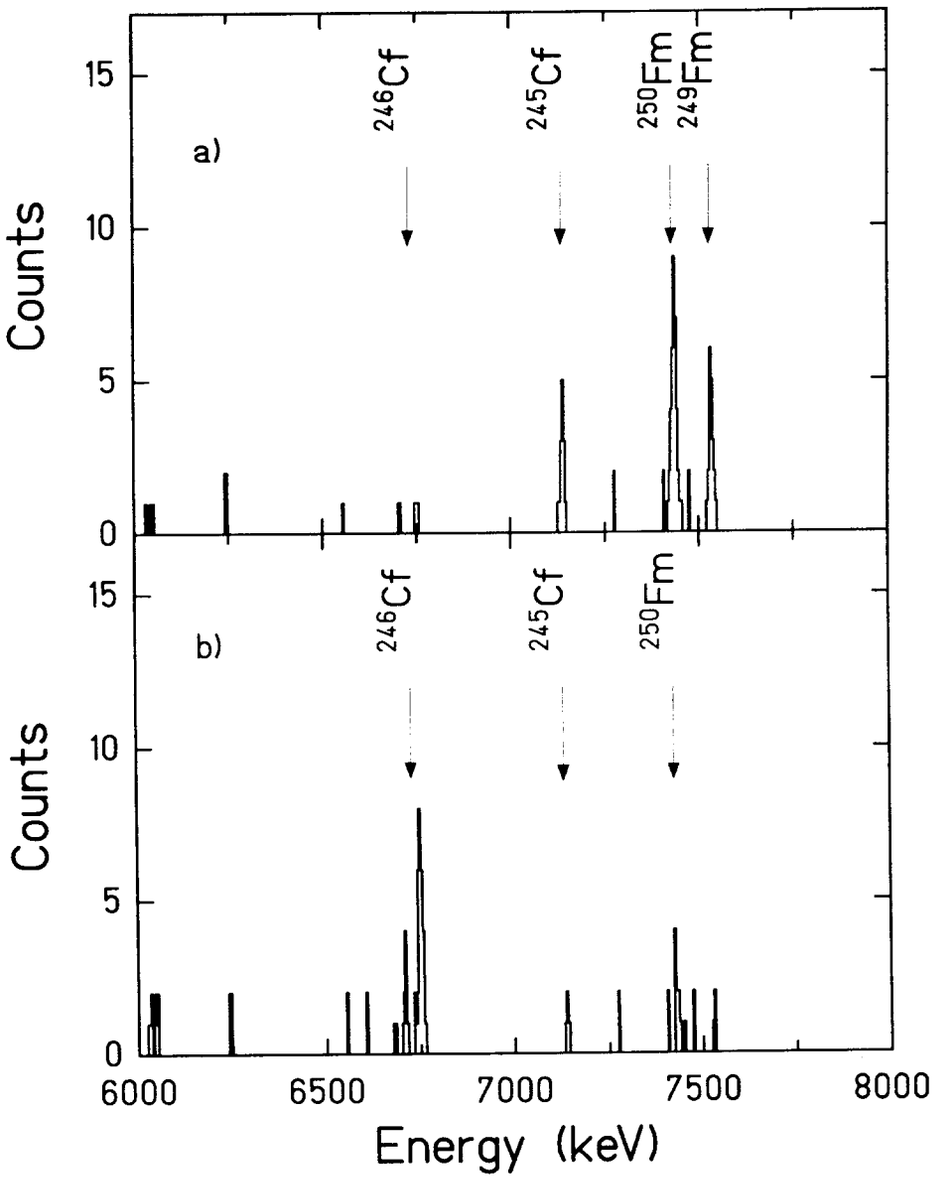

Figure 9: Energy spectrum of decay of implanted particles obtained in the reaction ^{238}U(^{16}O,xn)$^{254-xn}$Fm. Only particles outside the beam pulses are accumulated without correlation. The lower spectrum is accumulated during $\sim$ 30 hours after the irradiation.

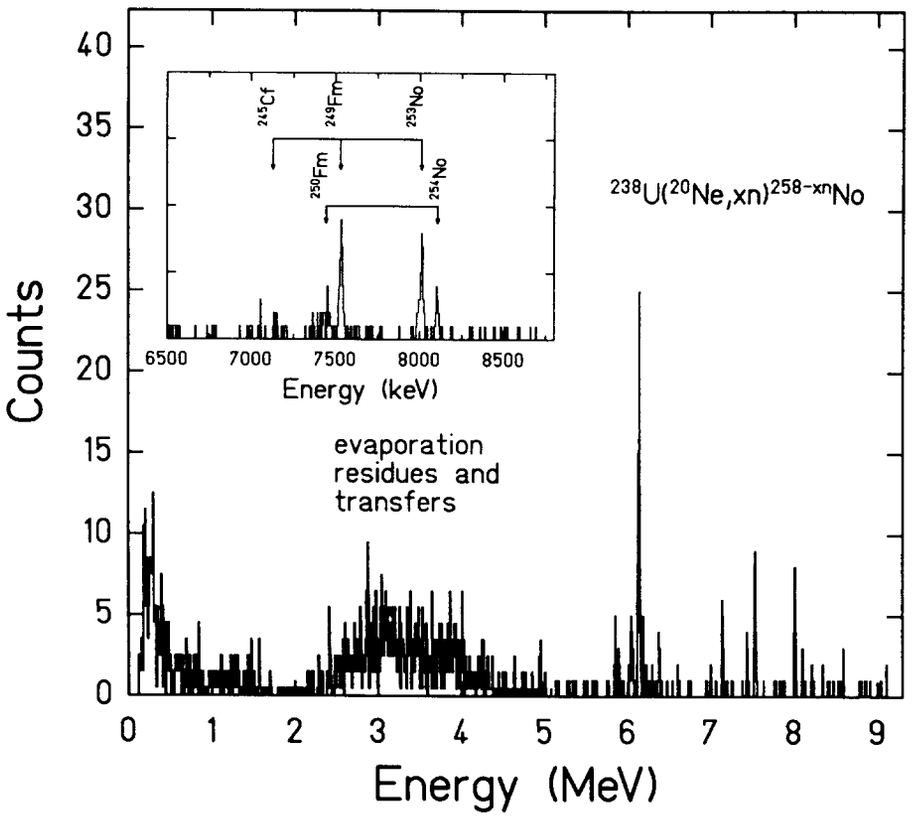

Figure 10: Energy spectrum obtained in the reaction $^{238}U(^{20}Ne,xn)^{258-xn}No$. In the inset only counts outside the beam-pulses are taken.